NANO LETTERS

2009
Vol. 9, No. 11
3853-3859

Rectification of the Ionic Current through Carbon Nanotubes by Electrostatic Assembly of Polyelectrolytes

Neal R. Scruggs,[†] Joseph W. F. Robertson,*[,‡] John J. Kasianowicz,[‡] and Kalman B. Migler*[,†]

Polymers Division, National Institute of Standards and Technology, Gaithersburg, Maryland 20899, Semiconductor Electronics Division, National Institute of Standards and Technology, Gaithersburg, Maryland 20899

Received June 26, 2009; Revised Manuscript Received August 6, 2009

ABSTRACT

Rectification of the ionic current flowing through nanotubes embedded in a polymeric membrane is achieved by selective adsorption of polycations to the nanotubes' mouths. A one-dimensional model of ionic flux through a nanotube with charged entrance regions qualitatively describes current−voltage curves before and after polycation exposure; reversal potential measurements confirm that charge reversal takes place upon polycation adsorption. The inherent simply of this electrostatic approach makes it attractive in membrane and nanofluidic applications employing rectification.

Advances in nanofabrication technologies over the past several years have enabled the emergence of nanofluidics as a distinct discipline.[1] Phenomena which often play a negligible role on a larger scale, such as volume exclusion, hydrophobic interactions, and electrostatic interactions, can dominate the transport of fluids through channels with dimensions on the order of nanometers,[2] and these unique effects can be exploited for a variety of applications such as single-molecule analysis[3−7] or separation processes.[8−10] Especially in the latter case, nanochannels exhibiting asymmetric conduction (i.e., nanofluidic diodes) are fundamental to the design of functional systems.

Numerous theoretical and experimental studies, as reviewed by Siwy,[11] have demonstrated that breaking symmetry either with respect to geometry or surface charge distribution leads to rectification of the ionic current through a nanopore. Theoretical modeling of nanochannels with inhomogeneous spatial distribution of electrostatic charge predicts diode-like behavior of the ionic flux.[9,12,13] Ionic current rectification has been observed experimentally in nanochannels fabricated by patterning their surfaces with charged molecules[14] and in asymmetrically modified carbon nanotube membranes having charged groups attached on only one side.[15−17] Experiments demonstrating ionic rectification in conical nanopores provide an example exploiting geometric asymmetry[18] or, by patterning their surfaces with charged moieties, the combination of geometric and charge asymmetry in a single system.[19]

Here we use a simple electrostatic assembly process to break charge symmetry in a nanoporous membrane leading to immediate rectification of the ionic current. Multiwalled carbon nanotubes dispersed in a polystyrene matrix serve as channels for ionic conductance and also provide targets for selective adsorption of charged polyelectrolytes at the pore mouths. We demonstrate that modifying only one side of the membrane yields nanochannels with high charge density localized to the entrance region, dramatically modifying the current−voltage characteristics of the membrane.

The multiwalled carbon nanotubes (MWCNTs) used in this study were obtained from Pyrograf Products Inc. (Cedarville, OH) and were selected on the basis of the following two criteria: we required the sample to have a large fraction of nanotubes with lengths of 1 μm or longer and with continuous, hollow cores so as to allow the uninterrupted transport of fluid. The latter may be hindered by residual catalyst particles and "bamboo-like" nanotubes present in the sample. According to the manufacturer's specifications the chosen product (Pyrograf-III PR-24-HT) contains CVD-grown carbon nanotubes with lengths ranging

* To whom correspondence should be addressed. (J.W.F.R.) E-mail: joseph.robertson@nist.gov. Phone: (301) 975-2506. Fax: (301) 948-4081. (K.B.M) E-mail: kalman.migler@nist.gov. Phone: (301) 975-4876. Fax: (301) 975-4924.
[†] Polymers Division.
[‡] Semiconductor Electronics Division.

10.1021/nl9020683
Published on Web 09/16/2009

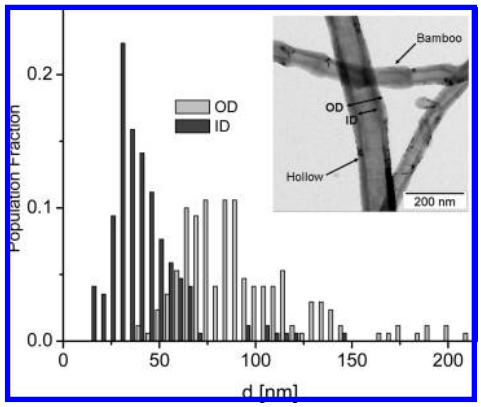

Figure 1. Histogram of inner (ID) and outer (OD) diameters measured from TEM images of 170 different MWCNTs. The inset TEM micrograph illustrates a typical hollow nanotube as well as a rare bamboo-like nanotube.

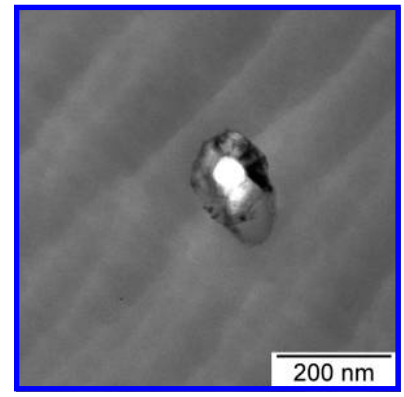

Figure 2. TEM micrograph of a hollow carbon nanotube with the axis oriented nearly perpendicular to the membrane surface. The nanotube is embedded in a polystyrene membrane 1 μm thick.

from 30 to 100 μm and diameters between 60 and 100 nm, subjected to a 3,000 °C heat treatment that effectively removes iron catalyst particles leftover from their synthesis. (Certain commercial materials and equipment are identified in this paper in order to specify adequately the experimental protocol. In no case does such identification imply recommendation by the National Institute of Standards and Technology, nor does it imply that such material or equipment identified is necessarily the best available.)

We measured the dimensions and open structure of the nanotubes using transmission electron microscopy (TEM). Approximately 2 mg of MWCNTs was dispersed in dimethylformamide (DMF) (~20 mL) by 4 h of bath sonication, then the suspension was dropped onto a carbon-coated TEM grid and dried on filter paper. These grids were imaged on a Philips EM400T transmission electron microscope operating at 120 kV and the inner and outer diameters of 170 different nanotubes were measured directly from the micrographs using ImageJ[20] (Figure 1). More than 95% of the nanotubes had an inner diameter between 15 and 65 nm with 50% of the population narrowly distributed between 30 and 40 nm and a few as large as 145 nm. Seventy percent of the measured nanotubes had an outer diameter between 60 and 100 nm; the smallest and largest tubes had outer diameters of 40 nm and 210 nm, respectively. The vast majority of MWCNTs imaged had hollow cores with a small minority having periodically walled-off "bamboo-like" structure (Figure 1, inset). Most of the MWCNTs observed were shorter than the specification, which is to be expected, because sonication tends to fragment carbon nanotubes. Nevertheless their lengths were typically at least a few micrometers (Supporting Information Figure 1).

Nanoporous polymeric membranes were prepared by dispersing MWCNTs in polystyrene (PS) then cutting thin sheets from the MWCNT/PS composite. A similar technique has been used to prepare membranes containing a single carbon nanotube pore.[21,22] TEM confirmed that nanotubes capable of transporting fluid across the membrane (i.e., hollow nanotubes with axes oriented roughly perpendicular to the membrane surface) are indeed present in the samples (Figure 2). Electron diffraction patterns confirm that structures such as that shown in Figure 2 are in fact nanotubes (Supporting Information, Figure 2). Composites were prepared using a solution blending process designed to yield well-dispersed MWCNTs within the polystyrene matrix.[23] MWCNTs were suspended in DMF at a weight fraction of approximately 2×10^{-5} by 4 h of bath sonication and then combined with a polystyrene/DMF solution (approximately 10% mass fraction PS), followed by another 4 h of sonication. The mixture was precipitated into ten times its volume of water by dropwise addition with vigorous stirring and, finally, the precipitate was dried in vacuum at approximately 150 °C for 24 h. The resulting composite, having a nanotube mass fraction of 2.9×10^{-6}, was melt-pressed at 180 °C into 1 mm thick sheets, from which membranes measuring approximately 0.5 mm × 0.5 mm × 1 μm were cut using a Leica Ultracut UCT microtome equipped with a histological diamond knife.

Voltammetric experiments were performed with a MWCNT-containing membrane separating two reservoirs of aqueous salt solution. An individual membrane was fixed to a PTFE support using a fast-curing silicone in a multistep procedure that limits its exposed area to a pinhole approximately 150 μm in diameter (see Supporting Information for details). A PTFE cell was assembled in which the supported membrane was mounted in between two 2.5 mL chambers, each equipped with a magnetic stir bar and a sealed Ag/AgCl electrode filled with 3 M KCl and separated from the bulk solution with a Vycor frit (Bioanalytical Systems, West Lafayette, IN). After assembly, the two reservoirs were filled with TRIS-buffered aqueous KCl (pH = 7) containing a nonionic surfactant (0.01% Triton-X 100) and the electrodes were connected to an Axon 200B patchclamp amplifier (Molecular Devices, Sunnyvale, CA). The purpose of adding Triton-X 100 was to accelerate wetting of the nanotube pores, and because it is nonionic it did not influence electrostatic assembly. Ionic current through the membrane was typically established immediately upon filling the solution reservoirs. No ionic current was observed when control experiments were performed using PS membranes that did not contain nanotubes.

The process of cutting carbon nanotubes to prepare a membrane creates broken carbon−carbon bonds that oxidize with exposure to the atmosphere creating ionizable chemical

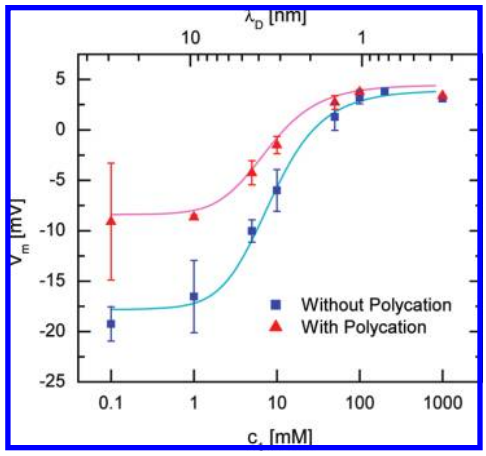

Figure 3. Reversal potential, V_m, as a function of electrolyte concentration, c_1, and Debye length, λ_D, at fixed concentration gradient ($c_2/c_1 = 2$) before (blue square) and after (red triangle) the addition of polycation. Solid lines are drawn to guide the eye. Error bars represent the standard deviations of multiple measurements on two distinct membranes.

functionalities on the exposed nanotubes' ends.[24,25] A similar strategy has been employed by other researchers using oxygen plasma etching to introduce carboxylic acid functionalities at the nanotubes' mouths.[16,17] Atmospheric oxidation though much milder should nevertheless be effective in introducing at least a small number of carboxyl groups that ionize in an aqueous environment to yield negative charges at the nanotubes' ends.

The presence of negative charges on the nanotubes' mouths was confirmed using membrane potential measurements.[26−28] In these experiments, a concentration cell is constructed with the membrane fixed between electrolyte reservoirs of unequal concentration ($c_1 \neq c_2$). From the diffusion of ions along the resulting concentration gradient we define the reversal potential, V_M, as the transmembrane bias required to counterbalance the ionic flux and yield zero current. The membrane potential is the sum of a diffusion potential and two Donnan potentials at the reservoir-membrane interfaces; the diffusion potential is determined by the concentration gradient and the Donnan potentials arise from the partitioning of ions to counterbalance fixed charges on the membrane surface. Thus, in the case of an uncharged membrane, the reversal potential is strictly proportional to the ratio of c_1 to c_2, and in our experiment we kept this ratio constant in order to highlight the influence of membrane charge. We measured the reversal potentials of MWCNT/PS membranes while varying the concentration of KCl in the reservoirs from $c_1 = 0.1$ to 1000 mM, maintaining the ratio of $c_2/c_1 = 2$ (Figure 3). Both reservoirs were well stirred during the measurement to minimize the effects of local concentration gradients at the membrane surfaces. With decreasing salt concentration, the data move from a plateau at high salt (KCl concentrations greater than approximately 50 mM) through a steep transition region to a second plateau at concentrations less than approximately 1 mM. Under these experimental conditions, an uncharged membrane would yield the same reversal potential regardless of the electrolyte concentration, but we observe that V_M depends strongly on c_1 and attribute this to the influence of charges present on the oxidized nanotube ends.

From the reversal potential measurements, we can infer that charges are located near the nanotubes' mouths. In order to have an influence on ionic transport the distance between charged groups and membrane pores must be less than the Debye length, λ_D, expressing a limiting length for charge separation, which in these experiments is approximately 30 nm, at most. Therefore the strong dependence of V_M on c_1 indicates that charges are within this distance from the nanotubes' mouths. Transition points in the V_M versus c_1 curve are approximately consistent with the geometry of the nanotubes; at 1 mM KCl, λ_D is comparable to the typical nanotube's diameter (on the order of 10 nm), while it is less than 2 nm for concentrations greater than 50 mM KCl. Charged groups influence membrane transport most at low concentrations, but are effectively screened by electrolyte when c_1 is large.

Charged groups fixed at the nanotubes' mouths also affect the cut membranes' current−voltage ($I-V$) characteristics. Filling both reservoirs with the same electrolyte solution, $I-V$ curves were measured from one MWCNT/PS membrane using various concentrations of KCl from 1 to 100 mM (Figure 4a−c) and in every case, nearly ohmic behavior was observed when the magnitude of the bias voltage was ≤200 mV. However, at higher potentials the $I-V$ curves deviate from linearity in a manner consistent with a negatively charged membrane. The number of conducting nanotubes in the sample, N, can be estimated from the membrane conductance, G, taken as the slope of the $I-V$ curve in the ohmic region. Modeling the nanotubes as ohmic conductors in parallel, we calculate G using the weighted average of individual nanotube conductances

$$G = N\sum_i x_i g_i \tag{1}$$

where

$$g_i = \frac{\pi d_i^2 \kappa}{4 l_i} \tag{2}$$

is the conductance of a single nanotube of diameter d_i and length l_i,[29] κ is the conductivity of the electrolyte, and x_i is the fraction of nanotubes of diameter d_i taken from the distribution in Figure 1. The calculated value of N depends on the salt concentration, but using the data at high salt (c = 50 mM and 100 mM) where charge effects should be minimal, we estimate the number of conducting nanotubes in the sample to be approximately 50.

The negative charges present at the nanotubes' mouths provide attractive sites for the electrostatic deposition of an oppositely charged polyelectrolyte. In an exceedingly simple process, a few microliters of polycation solution stirred into one of the electrolyte reservoirs coats the tips of the nanotubes with charged polymer and results in immediate rectification of the ionic current passing through the mem-

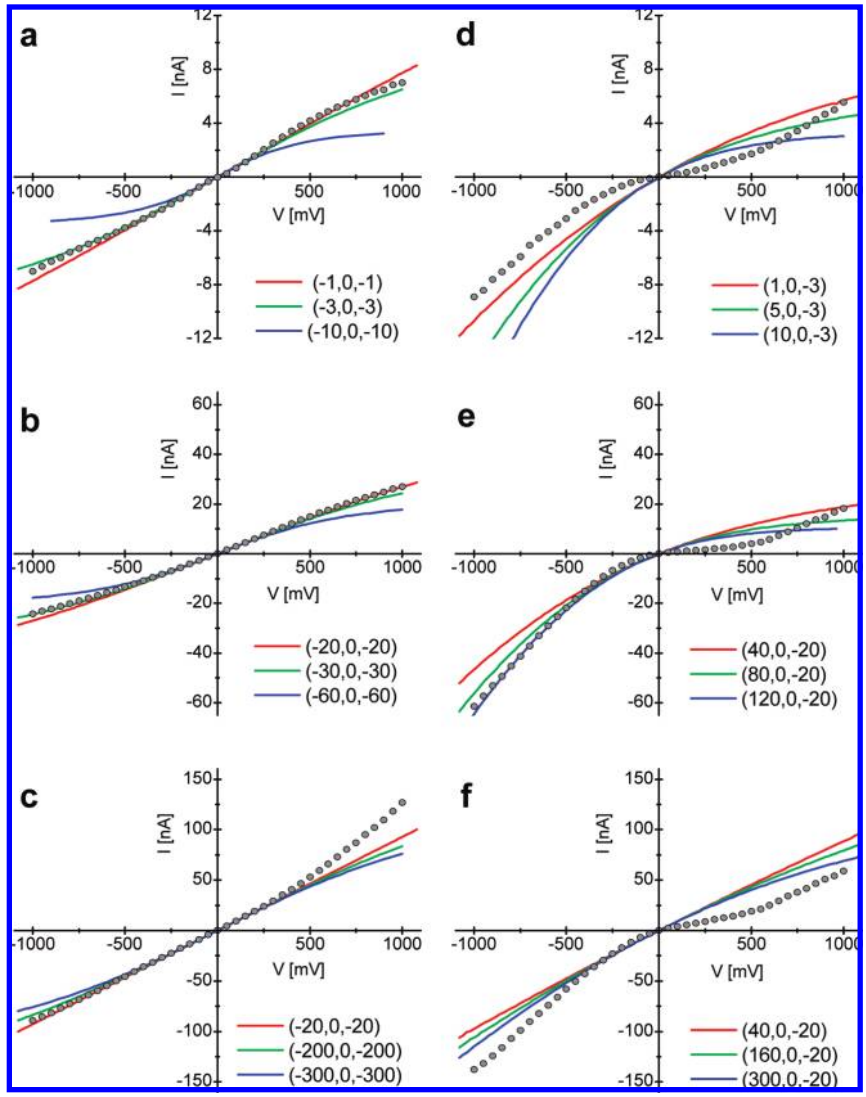

Figure 4. Current−voltage ($I-V$) curves before (a−c) and after (d−f) the addition of polycation in neutral, aqueous KCl solutions of various concentrations: (a,d) 1 mM, (b,e) 10 mM, and (c,f) 100 mM. Gray circles represent experimental data and solid lines are calculated from the one-dimensional model of a nanotube described in the text. The values of the surface charge densities in units of mC/m^2 are denoted in the legends as (σ_1, σ_2, σ_3).

brane. We envisage that the adsorbed polycation brings a relatively high density of fixed positive charges to the nanopores' mouths, which are balanced by highly mobile Cl^- counterions. Under forward bias, the chloride counterions are depleted causing the repulsion of K^+ ions and a reduction in the overall current. Under reverse bias, the mobile Cl^- counterions flow freely through the nanotube and the ionic current is enhanced.

The effect of electrostatic adsorption to the cut ends of the carbon nanotubes is readily apparent in the membranes' $I-V$ characteristics within minutes after adding a small amount of polycation to one side. Using the same membrane from which premodification $I-V$ curves were previously recorded, 5 μL of a 10 mg/mL aqueous solution of poly(dimethylamine-*co*-epichlorohydrin) was added to the nongrounded electrolyte reservoir and $I-V$ curves were remeasured approximately 10 min after a short (~3 s) burst of stirring. The postpolycation $I-V$ curves exhibit rectification of the ionic current with enhanced conductance at negative potentials and reduced conductance at positive potentials (Figure 4d−f).

Contrary to what is typically observed in nanofluidic diodes the rectification ratio, R, defined as the magnitude of the reverse-bias current divided by forward-bias current, exhibits a maximum both as a function of bias voltage and of salt concentration (Figure 5). Increasing the KCl concentration from 1 to 100 mM causes the R versus $|V|$ curve to shift first upward (between 1 mM and 10 mM) and then downward as c is further increased. This trend is qualitatively similar to observations made by Karnik et al.,[14] who noted negligible rectification through their nanofluidic diode at both very low ($c < 1$ mM) and very high ($c > 100$ mM) salt, the latter of which is expected due to charge screening effects. A unique feature of our data is that R reaches a maximum at approximately $|V| = 450$ mV regardless of the salt concentration, though the source of this phenomenon is not

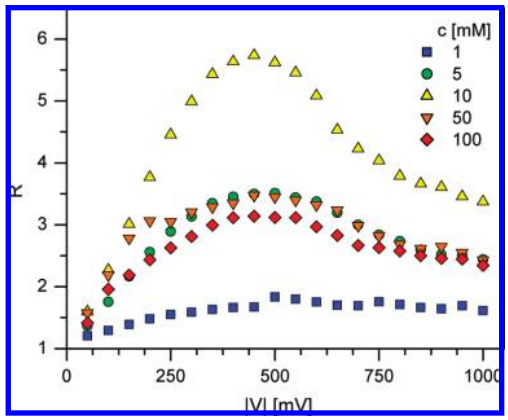

Figure 5. Rectification ratio, $R = |I(V_-)/I(V_+)|$, as a function of the magnitude of the bias voltage, V, at various salt concentrations, c. The uncertainty in R is approximately 30% based on repeated measurements.

immediately clear. The magnitude of R (between approximately $1 < R < 6$) is not unusual when compared with other experimental systems where reported rectification ratios typically vary between approximately $R = 2$ and $R = 100$, depending on pH, salt concentration, and applied potential.[2,14,30]

Several control experiments were performed on polyelectrolyte-modified membranes to further validate the hypothesis that the polymer is electrostatically adsorbed to the carbon nanotubes. First the solution reservoir containing polycation was thoroughly flushed with fresh KCl buffer to wash away free polyelectrolyte and leave behind only that which is physically attached to the membrane. This process had no effect on the membrane's $I-V$ characteristics indicating that polyelectrolyte is robustly bonded. Next the two fluid reservoirs were thoroughly flushed with acidic KCl buffer at pH = 3, which is reasonably expected to be below the pK_a of charged groups on the nanotubes' mouths (pK_a of acidic functionalities on carbon nanotubes could be as low as 4.5 or perhaps as high as 9).[16] The change in pH eliminated ionic current rectification as expected when negatively charged sites become fully protonated and no longer electrostatically bond with the oppositely charged polyelectrolyte. In a final control experiment fresh, unmodified membranes were exposed to polyanions to prove that rectification is not caused by nonspecific adsorption of the polyelectrolyte. Polyanions poly(styrene sulfonate) and poly(acrylic acid) had no effect on the $I-V$ characteristics but two other polycations, poly(allyl amine) and poly(dimethylamine-*co*-epichlorhydrin-*co*-ethylenediamine), both induced diode-like behavior (Supporting Information Figure 6).

Membrane potential measurements were repeated after the addition of polycation to confirm the reversal of charge at the nanotube entrance that takes place upon adsorption (Figure 3). At high salt, the postmodification reversal potential is in good agreement with the premodification data, as expected in the regime where membrane charge is effectively screened by the electrolyte. At low salt, the reversal potential after polycation modification is shifted approximately +10 mV, consistent with the hypothesis of

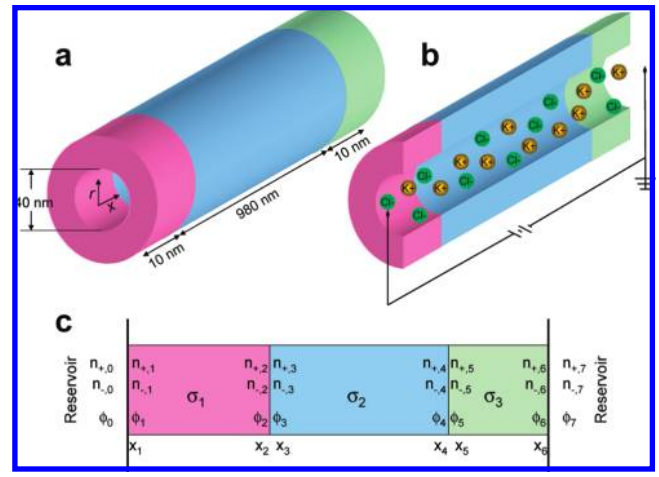

Figure 6. Schematic illustrations of the geometry used to model ionic flux through a nanotube with charged entrance and exit regions (drawings not to scale). (a) Schematic showing the coordinate system and dimensions of the nanotube. (b) Cutaway schematic illustrating ions flowing through the nanotube and also showing the orientation of the grounded electrode relative to the nanotube. (c) Schematic showing the nomenclature system used in modeling.

charge reversal on one side of the membrane. When both sides of the membrane carry negative fixed charge, the Donnan potentials at the reservoir-membrane interfaces are both reasonably expected to be negative. Changing one side of the membrane to bear positive charge reverses the sign of that Donnan potential, shifting the measured transmembrane potential to more positive values.

Experimentally measured $I-V$ curves were compared to calculations based on a one-dimensional model describing ionic flux through a nanotube with charged entrance regions (Figure 6). We model the ionic flux, J, of each species in a 1:1 electrolyte as the sum of a diffusive and an electophoretic flux. This model is essentially an approximate analytical, one-dimensional solution to the Poisson−Nernst−Planck equations,[19] and it has previously been used by Karnik et al. to describe rectification in a nanofluidic diode.[14] For a cylindrical tube with uniform diameter, d, and axial coordinate, x, the mass conservation equation is

$$J_{\pm} = D\frac{dn_{\pm}}{dx} \mp D\frac{F}{RT}n_{\pm}\frac{d\phi}{dx} \tag{3}$$

where D is the ionic diffusivity, n is the ion concentration, and φ is the electrical potential. We assume $D = 2 \times 10^{-5}$ cm^2/s for both K^+ and Cl^- ions.[31] Dividing the tube into three regions ($i = 1$, 2, and 3), each with uniform surface charge density, σ_i, eq 3 is solved subject to the electroneutrality condition

$$n_{+,i} - n_{-,i} + \frac{4\sigma_i}{Fd} = 0 \tag{4}$$

Donnan equilibrium is used to relate concentrations to electrical potentials at the reservoir/tube interfaces as well

as at the points of surface charge discontinuity within the tube itself:

$$\begin{aligned} \frac{n_{+,i}}{n_{+,i+1}} &= e^{F/RT(\phi_{i+1}-\phi_i)} \\ \frac{n_{-,i}}{n_{-,i+1}} &= e^{F/RT(\phi_i-\phi_{i+1})} \end{aligned} \tag{5}$$

Equations 3, 4, and 5 were solved numerically under a variety of different salt concentrations and surface charge conditions using Mathematica (Wolfram Research, Champaign, IL).

We set the tube length to 1 μm to be consistent with the membrane thickness. Polydispersity of tube diameters was taken into account by modeling tubes with $d = 20$, 40, 60, 80, 100, and 130 nm then performing a weighted summation using weighting factors derived from the measured distribution of inner diameters (Figure 1). We limit the length of the entrance and exit regions to 10 nm each in order to model fixed charges present only at the nanopore's mouths (Figure 6a); the surface charge density of the 980 nm central region is set to $\sigma_2 = 0$. After generating results with the single-tube model, we bring the calculation into registration with the experimental data through a multiplicative factor, N, equivalent to modeling N identical nanotubes in parallel.

Though it fails to reproduce the data exactly, this simple model does qualitatively explain the observed change in $I-V$ characteristics with polycation exposure (Figure 4). Theoretical $I-V$ curves were generated for electrolyte concentrations of 1, 10, and 100 mM using surface charge conditions that simulate carbon nanotubes before and after the adsorption of polycation. In the former case both ends of the tube are assigned small, negative charges ($\sigma_1 = \sigma_3 < 0$, $\sigma_2 = 0$) and in the latter case one end is changed to have a relatively large, positive charge ($\sigma_1 \gg 0$, $\sigma_2 = 0$, $\sigma_3 < 0$). The magnitudes of the surface charge densities were varied over a range of realistic values from 1 to 300 mC/m^2 (equivalent to 160 to 0.5 nm^2 of surface area per charged group) and, consistent with the experimental procedure, the positively charged end was always in contact with the nongrounded electrolyte reservoir. The premodification model (both ends carrying negative charges) produces $I-V$ curves that are symmetric about the origin and ohmic at small bias voltages. Imposing the postmodification condition (one end positively charged), the model produces diode-like behavior with current reduction at positive potentials and current enhancement at negative potentials. The gross features of the experimental results are thus well described by a very simple model for ionic flux through a nanotube.

The best quantitative agreement with experimental data was achieved at 10 mM salt. Modeling 132 nanotubes in parallel with $\sigma_1 = \sigma_3 = -20$ mC/m^2 yields excellent quantitative agreement with the premodification experimental $I-V$ curve (Figure 4b). Changing the surface charge density of the entrance region to $\sigma_1 = 80$ mC/ m^2 roughly reproduces the postmodification data (Figure 4e). The upturn of the experimental $I-V$ curve at high, positive voltages is a particularly notable feature that is not captured by the model. This feature recapitulates the unusual voltage-dependence of the rectification ratio noted earlier (Figure 5) and the model's failure to capture it emphasizes the need for a better understanding of its origin.

The theoretical model's ability to match experimental data at other salt concentrations is poor. At 1 mM salt the model accurately describes premodification data, though only when the surface charge is reduced to $\sigma_1 = \sigma_3 = -3$ mC/m^2 (Figure 4a). The postmodification $I-V$ curve exhibits greater enhancement of the reverse-bias current than is observed experimentally and fails to capture the reduction in current that is observed at low, positive voltages (Figure 4d). Increasing the salt concentration to 100 mM the premodification data is reasonably well modeled with a surface charge of $\sigma_1 = \sigma_3 = -20$ mC/m^2 except for an asymmetric upturn under forward bias that is probably attributable to a slight concentration gradient across the membrane resulting from incomplete flushing with 100 mM solution (Figure 4c). In order to model postmodification data, the magnitude of the entrance region's surface charge must be increased beyond the physically reasonable limit of $\sigma_1 = 300$ mC/ m^2 (Figure 4f).

Clearly this simple physical model does not describe all of the phenomena contributing to our experimental observations. Perhaps most notably, eqs 3, 4, and 5 predict an increase of baseline conductance (i.e., the slope of the $I-V$ curve in the low-bias, ohmic region) in direct proportion to salt concentration whereas our data exhibits a nonlinear relationship between the two. Because of this nonlinearity, a different multiplicative factor, N, must be used to model each set of experimental data: $N = 351$ for 1 mM KCl, $N = 132$ for 10 mM KCl, and $N = 41$ for 100 mM KCl (Supporting Information Figure 7). Furthermore, an accurate model should be able to describe data from different salt concentrations using the same values of the surface charge density, but we found it necessary to change the values of σ_1 and σ_3 from one data set to the next. Because of these shortcomings it is important to note that quantitative information such as the values of surface charge density cannot be extracted from our model. In order to model the data more precisely, it may be necessary to include effects such as electroosmotic flow or to carefully model the nanotubes' entrance regions. Furthermore, the labile nature of electrostatic bonds (i.e., the possibility for polyelectrolytes to reversibly detach from the nanotubes) may need to be accounted for in order to accurately describe our system.

In summary, our data supports the hypothesis that electrostatic assembly of polycation on the oppositely charged entrances to fluid-conducting carbon nanotubes leads to ionic selectivity and, therefore, rectification of the ionic current. In this work, we have demonstrated a facile means for dramatically modifying the transport of electrolytes through a nanoporous membrane by taking advantage of properties unique to carbon nanotubes. The charged groups that are introduced in the process of cutting the nanotubes are a critical component because they provide specific targets for polycation adsorption and the rectification effect we demonstrate relies on the polyelectrolyte's cluster of charges being brought into localized contact with the nanopores'

mouths. An advantage of our approach is that the carbon nanotubes can be manipulated with bench-scale processes like solution blending and microtoming, negating the need for complex nanofabrication techniques to construct our nanochannels. The electrostatic assembly strategy is attractive because it is simple enough to be adapted to any nanofluidic system employing carbon nanotubes or other types of charged nanochannels.

Acknowledgment. This research was conducted while N.R.S held a National Research Council Postdoctoral Research Associateship. J.J.K. was supported by the NIST Office of Law Enforcement Standards.

Supporting Information Available: Details regarding materials and methods, real-time voltammetric data taken during polycation modification, data from polyanion control experiments, and plot of membrane conductance versus salt concentration. This material is available free of charge via the Internet at http://pubs.acs.org.

References

(1) Abgrall, P.; Nguyen, N. T. *Anal. Chem.* **2008**, *80*, 2326.
(2) Vlassiouk, I.; Siwy, Z. S. *Nano Lett.* **2007**, *1*, 552.
(3) Ashkenasy, N.; Sanchez-Quesada, J.; Bayley, H.; Ghadiri, M. R. *Angew. Chem., Int. Ed.* **2005**, *44*, 1401.
(4) Ito, T.; Sun, L.; Crooks, R. M. *Chem. Commun.* **2003**, 1482.
(5) Kasianowicz, J. J.; Brandin, E.; Branton, D.; Deamer, D. W. *Proc. Natl. Acad. Sci. U.S.A.* **1996**, *93*, 13770.
(6) Robertston, J. W. F.; et al. *Proc. Natl. Acad. Sci. U.S.A.* **2007**, *104*, 8207.
(7) Storm, A. J.; et al. *Nano Lett.* **2005**, *5*, 1193.
(8) Murphy, R.; Muthukumar, M. *J. Chem. Phys.* **2007**, *126*, 051101.
(9) Ramirez, P.; Gomez, V.; Cervera, J.; Schiedt, B. *J. Chem. Phys.* **2007**, *126*, 194703.
(10) Siwy, Z. S.; Fulinski, A. *Phys. Rev. Lett.* **2002**, *89*, 198103.
(11) Siwy, Z. S. *Adv. Funct. Mater.* **2006**, *16*, 735.
(12) Daiguji, H.; Oka, Y.; Shirono, K. *Nano Lett.* **2005**, *5*, 2274.
(13) Neumcke, B. *Biophysik* **1970**, *6*, 231.
(14) Karnik, R.; et al. *Nano Lett.* **2007**, *7*, 547.
(15) Majumder, M.; Zhan, X.; Andrews, R.; Hinds, B. J. *Langmuir* **2007**, *23*, 8624.
(16) Majumder, M.; et al. *J. Membr. Sci.* **2008**, *316*, 89.
(17) Fornasiero, F.; et al. *Proc. Natl. Acad. Sci. U.S.A.* **2008**, *105*, 17250.
(18) Siwy, Z. S.; et al. *Europhys. Lett.* **2002**, *60*, 349.
(19) Vlassiouk, I.; Smirnov, S.; Siwy, Z. S. *Nano Lett.* **2008**, *8*, 1978.
(20) Abramoff, M. D.; Magelhaes, P. J.; Ram, P. J. *Biophotonics Int.* **2004**, *11*, 36.
(21) Ito, T.; Sun, L.; Crooks, R. M. *Anal. Chem.* **2003**, *75*, 2399.
(22) Sun, L.; Crooks, R. M. *J. Am. Chem. Soc.* **2000**, *122*, 12340.
(23) Du, F.; Fischer, J. E.; Winey, K. I. *J. Polym. Sci., Part B: Polym. Phys.* **2003**, *41*, 3333.
(24) Kónya, Z.; et al. *Chem. Phys. Lett.* **2002**, *360*, 429.
(25) Solhy, A.; et al. *Carbon* **2008**, *46*, 1194.
(26) Schaep, J.; Vandecasteele, C. *J. Membr. Sci.* **2001**, *188*, 129.
(27) Helfferich, F. *Ion Exchange*; McGraw-Hill: New York, 1962; pp 368−379.
(28) Hladik, J. *Physics of Electrolytes*; Academic Press: London, 1972; Vol. 1, pp 401−471.
(29) DeBlois, R. W.; Bean, C. P. *Rev. Sci. Instrum.* **1970**, *41*, 909.
(30) Alcaraz, A.; et al. *J. Phys. Chem. B* **2006**, *110*, 21205.
(31) Harned, H. S.; Nuttall, R. L. *J. Am. Chem. Soc.* **1949**, *71*, 1460.

NL9020683